2015

Highly Transparent Conductive Electrode with Ultra-Low HAZE by Grain Boundary Modification of Aqueous Solution Fabricated Alumina-Doped Zinc Oxide Nanocrystals

Qiong Nian

Michael J. Callahan

David C. Look
Wright State University - Main Campus, david.look@wright.edu

Harry Efstathiadis

John Bailey

See next page for additional authors

APL MATERIALS **3**, 062803 (2015)

Highly transparent conductive electrode with ultra-low HAZE by grain boundary modification of aqueous solution fabricated alumina-doped zinc oxide nanocrystals

Qiong Nian,[1] Michael Callahan,[2] David Look,[3] Harry Efstathiadis,[4] John Bailey,[2] and Gary J. Cheng[1]
[1]*Birck Nanotechnology Center and School of Industrial Engineering, Purdue University, West Lafayette, Indiana 47906, USA*
[2]*Greentech Solutions, Inc., Hanson, Massachusetts 02341, USA*
[3]*Semiconductor Research Center, Wright State University, Dayton, Ohio 45435, USA*
[4]*College of Nanoscale Science and Engineering (CNSE), University of Albany, Albany, New York 12203, USA*

(Received 30 December 2014; accepted 6 March 2015; published online 9 April 2015)

Commercial production of transparent conducting oxide (TCO) polycrystalline films requires high electrical conductivity with minimal degradation in optical transparency. Aqueous solution deposited TCO films would reduce production costs of TCO films but suffer from low electrical mobility, which severely degrades both electrical conductivity and optical transparency in the visible spectrum. Here, we demonstrated that grain boundary modification by ultra-violet laser crystallization (UVLC) of solution deposited aluminium-doped zinc oxide (AZO) nanocrystals results in high Hall mobility, with a corresponding dramatic improvement in AZO electrical conductance. The AZO films after laser irradiation exhibit electrical mobility up to 18.1 $cm^2 V^{-1} s^{-1}$ with corresponding electrical resistivity and sheet resistances as low as 1×10^{-3} Ω cm and 75 Ω/sq, respectively. The high mobility also enabled a high transmittance (T) of 88%-96% at 550 nm for the UVLC films. In addition, HAZE measurement shows AZO film scattering transmittance as low as 1.8%, which is superior over most other solution deposited transparent electrode alternatives such as silver nanowires. Thus, AZO films produced by the UVLC technique have a combined figure of merit for electrical conductivity, optical transparency, and optical HAZE higher than other solution based deposition techniques and comparable to vacuumed based deposition methods. [http://dx.doi.org/10.1063/1.4915489]

Transparent conducting films (TCFs) and transparent conductive electrodes (TCEs), materials that have both high electrical conductivity and optical transparency, are critical in many large consumer devices such as touch panels, displays, photovoltaic cells, and smart windows. Until recently, TCFs and TCEs were composed of transparent conducting oxides (TCOs) such as indium tin oxide (ITO), aluminium-doped zinc oxide (AZO), gallium doped zinc oxide (GZO), and other TCOs formed by vacuum techniques such as sputtering.

Increasingly, there is a desire for printable electronics for lower cost and more environmentally benign production methods. Considerable effort has been made in the R&D community to develop solution deposition processes that produce TCFs and TCEs that have high figure of merits of combined high optical transparency and electrical conductance.[1–6] Additionally, for display applications, low optical scattering (HAZE) is required to provide pleasing visual appearance. Progress has been made on low electrical conductivity TCEs from sparsely printed metal nanowires, which in at the nanoscale have low optical transparency, but effectively have high transparency with respect to human vision on the bulk scale.[7,8] Unfortunately, printed metal nanowires' inks are expensive at the production scale and suffer from high HAZE which is detrimental in display applications. Metal grids are also a promising technology but are difficult to print with feature sizes small enough

to effectively make the grids invisible to the naked eye.[7] Additionally, although proven viable for touch panels, metal nanowires and grids have not as yet been applied to TCFs in the display module itself. Current printed TCOs, such as ITO, AZO, and GZO, suffer from low electronic mobility, high porosity, and non-uniformity causing low electrical conductivity, optical scattering, and visible imperfections, thus are not satisfactory for touch panel or display applications.[9] Additionally, there is an intense investigation to develop a TCO to replace ITO which has the best combination of high mobility, high electrical conductivity (low sheet resistance), and high optical transparency in the visible (~400-700 nm).[10] Indium is a rare and expensive material used in many large consumer applications (solid state lighting, light-emitting diodes to backlight liquid-crystal displays, solar cells, and indium based thin-film-transistors). Replacing ITO with an indium free TCO would alleviate supplies constants for indium for other optoelectronic devices with large consumer markets. Therefore, there is a need for printed TCOs composed of predominantly abundant inexpensive elements with high optical transparency, low optical HAZE, and high electrical conductivity.

The alternative zinc oxide (ZnO) thin films have significant advantages such as chemical stability in reducing environments and the ability to dope with a wide range of elements.[11,12] Furthermore, Al doping enhances electrical conductivity by inducing free charge carriers and also stabilizes electrical stability of the ZnO thin film by impeding the chemisorption of oxygen at exposed surfaces including grain boundaries.[13] Various deposition techniques are used to prepare high quality AZO film with resistivity under 10^{-3} Ω cm and visible transmittance over 85%, such as DC sputtering,[14] pulsed laser deposition (PLD),[15] Atomic layer deposition (ALD),[16] and chemical vapor deposition (CVD).[12] However, these high vacuum methods have inherent instrumental complexity, high investment costs, and limited industrial scalability.[10] Thus, there has been a high demand to develop low cost non-vacuum deposition with soft conditions and reduced processing complexity. A variety of solution based approaches have been tried to obtain good optoelectronic properties comparable to vacuum deposition techniques, but achieving a high electrical conductivity (~1000 S cm^{-1}) with transparency over 85%-90% at 550 nm and low optical HAZE less than 2% in solution based approaches has been unsuccessful to the authors' knowledge.

Industrial laser crystallization using large Excimer line lasers up to 0.75 M in length is used to convert amorphous silicon to high mobility polycrystalline silicon for the display industry.[17] Similar Excimer laser technology should be adaptable to printed metal oxide polycrystalline thin films to enhance free carrier mobility (resulting in increased electrical conductivity with minimal degradation in optical transparency), while also decreasing optical scattering (HAZE), and improving large scale uniformity on a production scale. Therefore, herein, ultra-violet laser crystallization (UVLC) was employed to modify the grain boundaries and lower inter-grain imperfections of spin coated AZO films on soda lime glass substrates. The UV Excimer Laser significantly decreased extended defect concentrations and minimized free carrier scattering centers, leading to higher carrier mobility, improved electrical conductivity (~1000 S cm^{-1}), and high optical transmittance and low HAZE.

AZO thin films were prepared by spin coating multiple layers from a precursor solution on soda lime glass substrates followed by annealing in air for each layer deposited. The precursor solution consisted of semiconductor grade ethanol in which zinc acetate dihydrate [$Zn(CH_3COO)_2 \bullet 2H_2O$] (0.4 M) was dissolved. Aluminum nitrate hexahydrate [$Al(NO_3)_3 \bullet 6H_2O$] was dissolved in an amount to yield 2% Al in relation to Zn. Diethanolamine [$NH(CH_2CH_2OH)_2$, DEA] (1 M) was added to the zinc acetate. The solution was heated to approximately 75 °C and stirred for 2 h and allowed to cool to room temperature. Soda lime glass slides, sectioned into well-designed substrate, were loaded into a Laurell WS-650 spin coater with an automatic dispenser unit. The precursor solution was dispensed onto each substrate couple of layers with substrate spinning for dispensation and then 3000 rpm for drying. After each layer dispensed, sample was evaporated and annealed to convert each precursor layer to AZO. The stacked AZO layers were subsequently placed in a tube furnace and heated in argon with 2% hydrogen gas for post-treatment (2 h at 425 °C). Then, the well-fabricated sample was placed in a chamber purged with nitrogen to reduce the partial pressure of oxygen for UVLC. A KrF Excimer laser (λ of 248 nm and τ of 25 ns) was scanning on target film with intensities ranged from 130 to 210 mJ cm^{-2} and pulse number (N) ranged from 50 to 150, corresponding to a total laser irradiation time of 1.25-3.75 μs.

Afterwards, the sample was selectively re-annealed in forming gas to remove any saw damage and evaporate any surface contamination. Field emission scanning electron microscopy (FESEM) was used to observe the surface morphology and cross section structure for specific laser settings. The crystal size histograms were also calculated from the surface FESEM images. Electrical resistivity, carrier mobility, and carrier concentration were measured by the Hall effect with the Van der Pauw method. Optical transmittance spectra and scattering were measured by a Lambda 950 ultraviolet-visible and infrared (UV-Vis-IR) spectrophotometer. Light scattering was quantified by HAZE measurement, which is stated by the difference between diffusive and specular transmittance (the light comes out of the sample parallel to the incident light).

Microstructure characterization by SEM was conducted to understand effects of laser crystallization on the grain structure changes in AZO thin film. A schematic illustration of grain enlargement from UVLC is shown in Figure 1(a) with corresponding FESEM plain view images before (Figure 1(b)), during (Figures 1(c) and 1(d)), and after (Figure 1(e)) UVLC of sol gel AZO films using a laser intensity of 172 mJ cm^{-2}. It can be seen in Figure 1(b), before UVLC, the as-coated AZO films possess a porous film structure with numerous defects including voids, gaps, grain boundaries, a discontinuous surface, and overall inhomogeneity.[18,19] Figures 1(b)-1(e) show a significant densification and coalescence films during and after UVLC with smaller grains merging into larger ones with distinct faceting and narrow grain boundaries. Small grains were enlarged by partial melting, merging, crystallizing, and finally impinging on each other during UVLC, forming a homogeneous and continuous film quality. This is demonstrated quantitatively by grain size distribution histograms (inset of

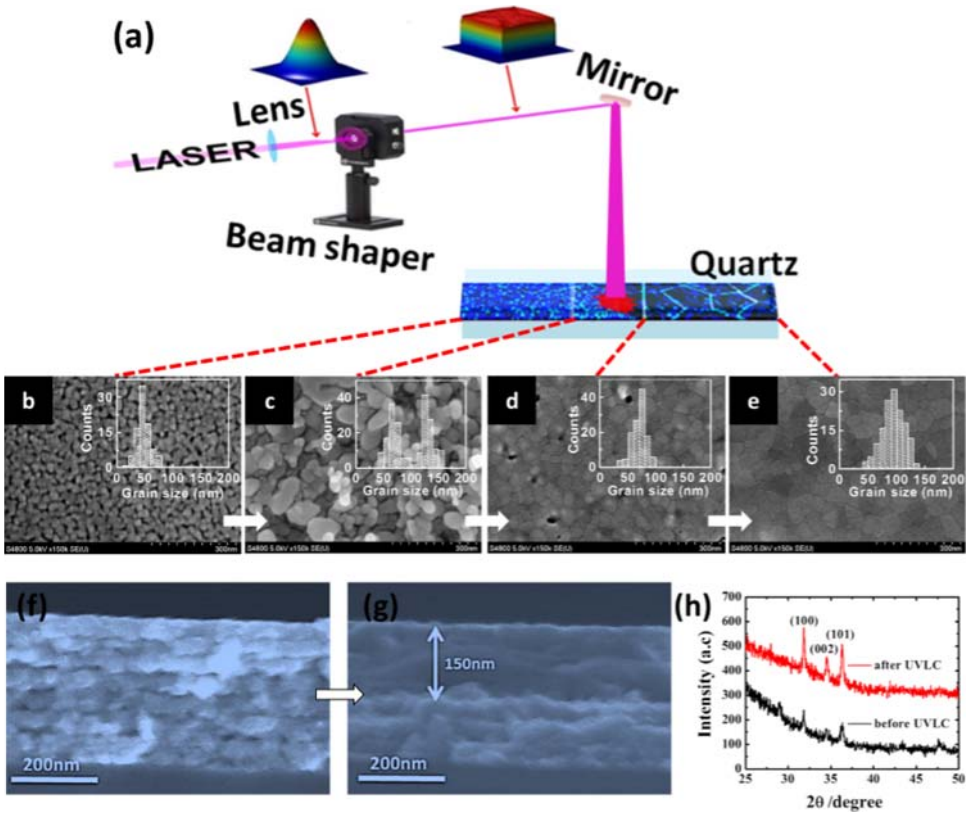

FIG. 1. UVLC influence on AZO film microstructure: (a) AZO film crystallization process scheme. Plane-view FESEM image of AZO film: (b) before UVLC; (c) during initial stage of UVLC when non-homogeneous particle melting of nanocrystals started; (d) during later stage of UVLC, large crystals are grown by merging of nanocrystals while still leaving porosity between crystals; (e) uniform and large crystals after UVLC. Inset: Grain size distribution in AZO film. (f) SEM cross section of spin coated AZO before LC showing uniform densification and a one layer structure; (g) SEM cross section image after UVLC clearly showing densification and a two layer structure; and (h) the XRD spectrum before and after laser crystallization of AZO nano-ink.

Figs. 1(b)-1(e)) during UVLC demonstrating reducing grain boundary densityafter UVLC. The grain size was measured by analyzing the SEM images. Reduced grain boundary density in combination with less inter-grain defects (voids, gaps, and discontinuities) would cause a corresponding reduction in electron traps, thus diminishing overall grain boundary barrier scattering increasing grain boundary mobility in post-UVLC films. Increased grain boundary mobility would increase the Hall mobility measured in the polycrystalline AZO film after UVLC, similar to vapor deposited AZO films with large oriented grain structure.[12,20,21] Cross section FESEM is shown before (Figure 1(f)) and after (Figure 1(g)) UVLC (172 mJ cm^{-2}). The XRD spectrum before and after laser crystallization of AZO nano-ink was shown in Figure 1(h). It can be seen that laser crystallization of thin film was increased significantly as the Width-Full Width at Half Maximum (FWHM) was reduced after laser crystallization. It is clearly seen in Figure 1(g) a thick top layer (~150 nm) of the AZO film was crystallized by UVLC which is denser and more fully crystallized than the bottom portion of the film. It is believed the top layer was formed primarily by melting while the bottom layer crystallized to a lesser degree due to rapid thermal dissipation limiting the temperature in the bottom layer to below the melting point of the AZO nanoparticles. The 248 nm UV laser only has an absorption depth of approximately 50 nm and in combination with the 25 ns pulse rate and 10 Hz duty cycle resulted in rapid cooling and a lower maximum peak temperature in the bottom layer causing grain densification primarily to occur from solid state annealing below the melting point. This is confirmed by numerical simulations that simulate the temperature of the film during high speed laser crystallization.[19,22,23] It is believed that the majority of increased mobility, improved carrier concentration, and corresponding electron flow are primarily in the denser, more uniform top layer. Further experimentation and modeling are being conducted to confirm a 2-layer model with a high mobility degenerate top layer and a lower mobility bottom layer and will be published in a future publication. Given the preceding discussion, UVLC processed AZO films' electrical measurements were calculated based on 150 nm top layer thickness.

Figure 2(a) shows the change in electrical properties of AZO films measured by Hall effect measurement. After the crystallization, a strong decrease in sheet resistance R_s and resistivity ρ_{hall}

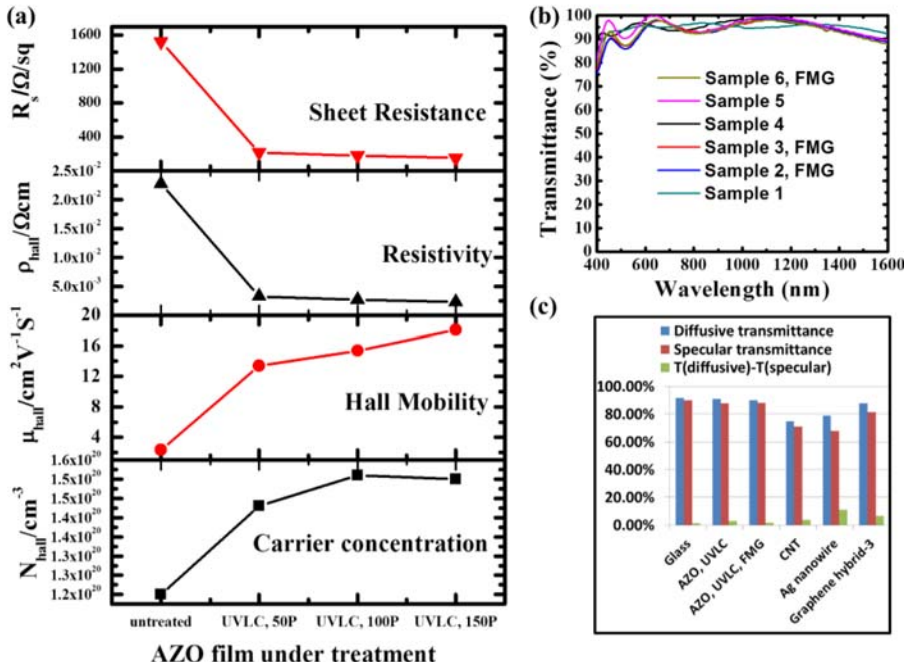

FIG. 2. (a) Pulse number dependence of Hall measurement employing UVLC with optimal fluence of 172 mJ cm^{-2}. Influence of UVLC on transmittance: (b) influence of UVLC parameters on AZO films UV-Vis-IR transmittance; (c) diffusive and specular transmittance of glass, CNT, silver nanowire, graphene, and AZO films. The difference in the diffusive transmittance and the specular transmittance plotted evaluates HAZE.

is observed for all different laser parameters. R_s decreases from 1.5 KΩ/sq to 217, 179, and 153 Ω/sq, respectively, when 50, 100, and 150 pulses were delivered to AZO film with fluence of 172 mJ cm^{-2}. ρ_{hall} decreases from 2.28×10^{-2} Ω cm to 3.26×10^{-3}, 2.69×10^{-3}, 2.30×10^{-3} Ω cm, respectively. The further investigation of carrier concentration and carrier mobility of the untreated and processed films is plotted in Figure 2(a). It can be seen that increase in conductivity is proportional to increase in carrier mobility, as well as a moderate increase in carrier concentration. Under optimal laser condition of 172 mJ cm^{-2} and 150 pulses, the solution based AZO thin film has a remarkably high mobility values of 18.1 cm^2 V^{-1} s^{-1} with a high carrier concentration of 1.50×10^{20} cm^{-3} leading to resistivity of 2.30×10^{-3} Ω cm.

Well known, polycrystalline AZO thin film Hall mobility is usually dominated by either ionized impurity scattering or grain boundary scattering, according to different carrier concentrations,[12,20,21,24] neglecting neutral impurity scattering, lattice vibration scattering, and intragrain cluster scattering.[24] For relative high carrier concentrations (>2×10^{20} cm^{-3}), the mobility is dominated by impurity ion scattering, since the traps between grains can be partially or completely filled, reducing grain boundaries scattering. For the relative low carrier concentrations (<2×10^{20} cm^{-3}) in this study, it is generally agreed that mobility is dominated by grain boundary scattering, which was determined by grain boundary density and energy potential barrier (Φ_B) at grain boundaries.[21,25] To describe the grain boundary mobility μ_g, Seto and Baccarani[26,27] extend Petriz model[28] in Eq. (1).

$$\mu_g = \mu_0 \exp\left(-\frac{\Phi_B}{kT}\right) = \frac{eL}{\sqrt{2\pi m^* kT}} \exp\left(-\frac{e^2 N_t{}^2}{8kT\varepsilon\varepsilon_0 N_{eff}}\right), \quad (1)$$

where L is the grain size, N_t is the electron trap density at grain boundaries, N_{eff} is the free electron concentration, m^* is the electron effective mass, $\varepsilon\epsilon_0$ is the static dielectric constant, and e is the elementary charge. After crystallization, grain size L is enlarged, with an increase factor of ~2 times according to Figures 1(e) and 1(f) histograms, which leave a large margin compared with the significant mobility increase factor of ~8 times (from 2.3 to 18.1 cm^2 V^{-1} s^{-1}). Thus, electron trap density N_t should have been lowered to achieve high mobility. Since extended defects like inter-grain voids, gaps, and grain boundaries might form electron traps at grain boundaries.[29] UVLC process forms facetted grains that impinge with each other to achieve compact structure, significantly lowering the internal defect density and contributing to electron trap density decrease. In addition, prior reports[10,12] also state that UV light exposure is capable to desorb oxygen species at grain boundaries, which help decrease electron trap density as well. Desorption of oxygen species would release free carriers from traps which could be demonstrated by a moderate increase of carrier concentration after UVLC shown in Figure 2(a). Both enlarged grain size and decreased electron trap density contribute to Hall mobility enhancement at low carrier concentration.

Annealing the post-processed UVLC samples in forming gas at 400 °C decreased the resistivity further as shown in Table I. Due to sample cutting with aqueous based slurry, surface contamination may have degraded the conductivity, as water and humidity are known to degrade the electrical properties of AZO, particularly at elevated temperatures which could have been introduced from saw friction during cutting. As compared, the sheet resistance R_s of AZO thin film drops from "150-280 Ω/sq" level to "75-95 Ω/sq" level after FMG (Forming gas treatment under 400 °C). Similarly, resistivity deceases from 2.69×10^{-3} Ω cm to 1.13×10^{-3} Ω cm. The sheet resistance drop and electrical resistivity decrease are mainly due to the contamination removal and free carrier release.[12] It was found

TABLE I. UVLC conditions on AZO films and the derived performance.

Sample	Laser intensity mJ cm^{-2}	Pulse number	FMG	R_{sheet} Ω/sq	Transmittance at 500 nm (%)
1	172	50	No	217	95
2[a]	172	100	Yes	75	88
3[a]	172	150	Yes	79	89
4	192	50	No	273	96
5	192	100	No	198	94
6[a]	192	150	Yes	95	88

[a]FMG: Forming gas treatment.

that the grain structure change before and after FMG is not obvious. During FMG annealing AZO thin film, the process mainly changed the oxygen species absorbed in grain boundary. The carrier density increase might influence carrier mobility, but not dominant; thus, a remarkable low sheet resistance is achieved by FMG following UVLC.

UV-Vis-IR transmittance was performed in Figure 2(b), illustrating the transmittance spectrum in the wavelength range of 400-1600 nm from samples in Table I. An uncoated soda lime glass substrate was used as a reference to calculate the transmission of the AZO films alone. All results meet the requirements of touch screen display for practical application (R_s: 500 Ω/sq; T: 85%). For instance, the films processed by 172 mJ cm^{-2} reach 217 Ω/sq with 95% T at 550 nm, 75 Ω/sq with 88% T at 550 nm, and 79 Ω/sq with 89% T at 550 nm, depending on laser pulse number and FMG, respectively. To the author's knowledge, low sheet resistance/high transparency (R_s < 80 Ω/sq; T > 88%) solution fabricated AZO films with post-treatment has not been reported before. This remarkable optoelectronic performance can be attributed to the relaxing increasing carrier mobility after UVLC.[10,12] The transmittance exhibits a slight decrease in the Vis-IR range after FMG owing to further released free carrier absorption.[10,12] In order to further investigate the potential of UVLC on macro-scale applications, HAZE measurement was carried out at 550 nm wavelength and compared with other transparent electrode alternatives,[7,30] as shown in Figure 2(c). It can be seen that the scattering of AZO film is ~2.7% after UVLC and ~1.8% after FMG, which implies the FMG process aided to improve film surface uniformity and homogeneity. Comparing with other alternatives like carbon nanotube (CNT) (~3%), silver nanowires (~10%), and graphene hybrid film (h3, ~6.6%), whose high light scattering scale might trigger problematic for certain displays like touch screens,[7] the accomplished film achieves significant low light scattering which has the potential to at or below the scattering in ITO (~1%).[7,30]

Figure 3(a) milestones the accomplished AZO film performance, comparing with experimental data for ITO thin films[31] and other recently developed transparent electrode alternatives such as CNT random meshes,[32–34] silver nanowire networks,[7] metal gratings,[35] and graphene.[30,36] The UVLC AZO films compare favorably to vapor deposited ITO and other transparent electrodes at a lower manufacturing cost due to the nature of printing technology. Figure 3(b) plots electron mobility vs. free electron concentration data for AZO thin films deposited with different process conditions from several groups.[10,12,37–46] These prior advancements have achieved high electrical conductivity on different substrates with vacuum or aqueous solution methods and provide a comparison with the work discussed here on UVLC aqueous solution AZO films (red curve in Figure 3(b)). The highest electrical conductivity of the UVLC series of sample reaches ~1000 S cm^{-1}, which performs better than the up-to-date best aqueous solution method[10] and many vacuum methods.[12,37,39,46] In addition,

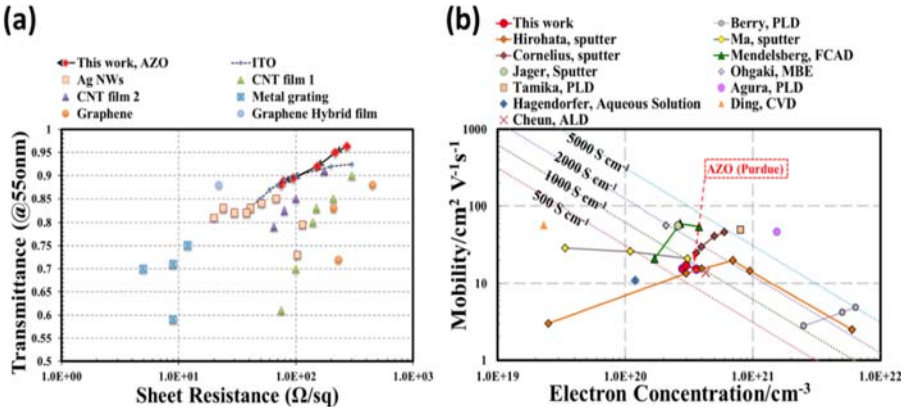

FIG. 3. (a) The performance of transmittance at 550 nm and sheet resistance for AZO films, comparing with ITO, CNT, silver nanowires, metal gratings, and graphene. (b) Electron mobility vs. electron concentration for AZO films processed by UVLC and FMG, comparing with high vacuum deposition by nine research groups. The red curve shows current work, the other marked points and curves represent high mobility AZO films listed for comparison. The diagonal dashed lines show constant conductivity on a log-log scale.

grain boundary density also could be affected by film thickness which would further influence the carrier mobility.[12]

In conclusion, the aqueous solution fabrication and following grain boundary modification by UVLC have been built to deposit transparent and conductive AZO films with better structural and optoelectronics properties than most high temperature/high vacuum deposition methods, suggesting a potential for low cost and large scale manufacturing. The grain boundary modification includes grain boundary density decrease and the electron trap density decrease at grain boundaries. Under optimal physical parameters, modified film with low resistivity of $\sim 1 \times 10^{-3}$ Ω cm, high Hall mobility of 18.1 $cm^2\ V^{-1}\ s^{-1}$, and low sheet resistance of 75 Ω/sq was obtained. The results of the current study including a measured sheet resistance of 75 Ω/sq with a corresponding transmission at 550 nm of 88% exceed the results of other aqueous solution deposition/post-treatments of AZO thin films to date. The light scattering of the AZO film exhibiting just 1.8% also suggests a potential to compete with market mainstream ITO film for display applications.

We sincerely thank the financial supports from US National Science Foundation through SBIR Phase I and Phase II.

[1] R. G. Gordon, MRS Bull. **25**(08), 52 (2000).
[2] K. Ellmer, Nat. Photonics **6**(12), 809 (2012).
[3] M. Girtan, Sol. Energy Mater. Sol. Cells **100**, 153 (2012).
[4] J.-A. Jeong, H.-K. Kim, and J. Kim, Sol. Energy Mater. Sol. Cells **125**, 113 (2014).
[5] S. B. Sepulveda-Mora and S. G. Cloutier, J. Nanomater. **2012**, 9.
[6] C.-H. Chung, T.-B. Song, B. Bob, R. Zhu, and Y. Yang, Nano Res. **5**(11), 805 (2012).
[7] L. Hu, H. S. Kim, J.-Y. Lee, P. Peumans, and Y. Cui, ACS Nano **4**(5), 2955 (2010).
[8] M.-H. Chang, H.-A. Cho, Y.-S. Kim, E.-J. Lee, and J.-Y. Kim, Nanoscale Res. Lett. **9**(1), 1 (2014).
[9] N. Al-Dahoudi and M. A. Aegerter, Thin Solid Films **502**(1–2), 193 (2006).
[10] H. Hagendorfer, K. Lienau, S. Nishiwaki, C. M. Fella, L. Kranz, A. R. Uhl, D. Jaeger, L. Luo, C. Gretener, S. Buecheler, Y. E. Romanyuk, and A. N. Tiwari, Adv. Mater. **26**(4), 632 (2014).
[11] D. Altamiranojuarez, Sol. Energy Mater. Sol. Cells **82**(1-2), 35 (2004).
[12] L. Ding, S. Nicolay, J. Steinhauser, U. Kroll, and C. Ballif, Adv. Funct. Mater. **23**(41), 5177 (2013).
[13] S. J. Pearton, D. P. Norton, K. Ip, Y. W. Heo, and T. Steiner, Prog. Mater. Sci. **50**(3), 293 (2005).
[14] W.-J. Jeong and G.-C. Park, Sol. Energy Mater. Sol. Cells **65**(1–4), 37 (2001).
[15] O. Bamiduro, H. Mustafa, R. Mundle, R. B. Konda, and A. K. Pradhan, Appl. Phys. Lett. **90**(25), 252108 (2007).
[16] N. P. Dasgupta, S. Neubert, W. Lee, O. Trejo, J.-R. Lee, and F. B. Prinz, Chem. Mater. **22**(16), 4769 (2010).
[17] R. Delmdahl and R. Pätzel, J. Phys. D: Appl. Phys. **47**, 034004 (2014).
[18] M. Y. Zhang and G. J. Cheng, Appl. Phys. Lett. **99**(5), 051904 (2011).
[19] M. Y. Zhang, Q. Nian, and G. J. Cheng, Appl. Phys. Lett. **100**(15), 151902 (2012).
[20] K. Ellmer, in *Transparent Conductive Zinc Oxide*, edited by K. Ellmer, A. Klein, and B. Rech (Springer, Berlin, Heidelberg, 2008), Vol. 104, p. 35.
[21] A. E. Delahoy and S. Guo, in *Handbook of Photovoltaic Science and Engineering* (John Wiley & Sons, Ltd., 2011), p. 716.
[22] Q. Nian, M. Y. Zhang, B. D. Schwartz, and G. J. Cheng, Appl. Phys. Lett. **104**, 201907 (2014).
[23] M. Y. Zhang, Q. Nian, Y. Shin, and G. J. Cheng, J. Appl. Phys. **113**(19), 193506 (2013).
[24] J. G. Lu, Z. Z. Ye, Y. J. Zeng, L. P. Zhu, L. Wang, J. Yuan, B. H. Zhao, and Q. L. Liang, J. Appl. Phys. **100**(7), 073714 (2006).
[25] T. Minami, MRS Bull. **25**(08), 38 (2000).
[26] J. Y. W. Seto, J. Appl. Phys. **46**(12), 5247 (1975).
[27] G. Baccarani, B. Riccò, and G. Spadini, J. Appl. Phys. **49**(11), 5565 (1978).
[28] R. L. Petritz, Phys. Rev. **104**(6), 1508 (1956).
[29] Z. Zhang, C. Bao, S. Ma, and S. Hou, Appl. Surf. Sci. **257**(17), 7893 (2011).
[30] R. Chen, S. R. Das, C. Jeong, M. R. Khan, D. B. Janes, and M. A. Alam, Adv. Funct. Mater. **23**(41), 5150 (2013).
[31] J.-Y. Lee, S. T. Connor, Y. Cui, and P. Peumans, Nano Lett. **8**(2), 689 (2008).
[32] G. Gruner, J. Mater. Chem. **16**(35), 3533 (2006).
[33] J. Li, L. Hu, L. Wang, Y. Zhou, G. Grüner, and T. J. Marks, Nano Lett. **6**(11), 2472 (2006).
[34] H.-Z. Geng, K. K. Kim, K. P. So, Y. S. Lee, Y. Chang, and Y. H. Lee, J. Am. Chem. Soc. **129**(25), 7758 (2007).
[35] M. G. Kang and L. J. Guo, Adv. Mater. **19**(10), 1391 (2007).
[36] L. G. De Arco, Y. Zhang, C. W. Schlenker, K. Ryu, M. E. Thompson, and C. Zhou, ACS Nano **4**(5), 2865 (2010).
[37] K. Hirohata, Y. Nishi, N. Oka, Y. Sato, I. Yamamoto, and Y. Shigesato, "High Rate Deposition of Al-doped ZnO by Reactive Sputtering: (1) Unipolar Pulsing with Plasma Emission Control," *Materials Research Society Symposium Proceedings*, Boston, Massachusetts, USA, 1-5 December 2008, Vol. 1109, p. 37.
[38] J. J. Berry, D. S. Ginley, and P. E. Burrows, Appl. Phys. Lett. **92**(19), 193304 (2008).
[39] G. Ma, D. Li, H. Ma, J. Shen, C. Wu, J. Ge, S. Hu, and N. Dai, Appl. Phys. Lett. **93**(21), 211101 (2008).
[40] S. Jäger, B. Szyszka, J. Szczyrbowski, and G. Bräuer, Surf. Coat. Technol. **98**(1–3), 1304 (1998).
[41] T. Ohgaki, Y. Kawamura, T. Kuroda, N. Ohashi, Y. Adachi, T. Tsurumi, F. Minami, and H. Haneda, Key Eng. Mater. **248**, 91 (2003).
[42] S. Cornelius, M. Vinnichenko, N. Shevchenko, A. Rogozin, A. Kolitsch, and W. Möller, Appl. Phys. Lett. **94**(4), 042103 (2009).

[43] H. Tanaka, K. Ihara, T. Miyata, H. Sato, and T. Minami, J. Vac. Sci. Technol., A **22**(4), 1757 (2004).
[44] H. Agura, A. Suzuki, T. Matsushita, T. Aoki, and M. Okuda, Thin Solid Films **445**(2), 263 (2003).
[45] R. J. Mendelsberg, S. H. N. Lim, Y. K. Zhu, J. Wallig, D. J. Milliron, and A. Anders, J. Phys. D: Appl. Phys. **44**(23), 232003 (2011).
[46] H. Cheun, C. Fuentes-Hernandez, J. Shim, Y. Fang, Y. Cai, H. Li, A. K. Sigdel, J. Meyer, J. Maibach, A. Dindar, Y. Zhou, J. J. Berry, J.-L. Bredas, A. Kahn, K. H. Sandhage, and B. Kippelen, Adv. Funct. Mater. **22**(7), 1531 (2012).